

Numerical Verification and Experimental Validation of Sliding Mode Control Design for Uncertain Thermal SOFC Models*

Andreas Rauh, Luise Senkel, Thomas Dötschel[†], Harald Aschemann
Chair of Mechatronics, University of Rostock,
Justus-von-Liebig-Weg 6, D-18059 Rostock, Germany
{Andreas.Rauh, Luise.Senkel, Harald.Aschemann}@uni-rostock.de

Ekaterina Auer
Faculty of Engineering, INKO, University of
Duisburg-Essen, D-47048 Duisburg, Germany
Auer@inf.uni-due.de

Abstract

The design of reliable and robust control strategies for the automatized operation of SOFC systems in a decentralized power grid demands for the use of nonlinear dynamic system models with a large number of physical parameters. These models have to cover the most dominant nonlinear effects and include knowledge about the uncertainty of specific parameters. In this paper, interval variables are taken into account to represent imperfect system knowledge during modeling on the one hand and to account for possible ambiguities in the system parameterization on the other hand. As soon as point values are chosen from parameter intervals identified by means of global optimization techniques in previous work, it becomes necessary to determine control laws which compensate the remaining uncertainties as well as non-modeled disturbances in a reliable way. For this purpose, guaranteed stabilizing control strategies are derived in this paper using the principle of sliding mode design. This methodology is extended towards a reliable interval-based implementation that can be evaluated in real-time environments. In such a way, it is possible not only to validate the resulting control strategies offline by means of simulations but also to use the same program code online on a real-life test rig. Corresponding experimental results are presented in this paper for an SOFC system that is available at the Chair of Mechatronics at the University of Rostock.

Keywords: Interval analysis, Lyapunov methods, robust control, sliding mode design, disturbance observers

AMS subject classifications: 65G20, 65G30, 93C15, 93C95, 37B25

*Submitted: February 10, 2013; Revised: May 26, 2014; Accepted: May 28, 2014

[†]Th. Dötschel was with the Chair of Mechatronics, University of Rostock, while this work was performed.

1 Introduction

The dynamic behavior of high-temperature solid oxide fuel cell systems (SOFC systems) can be described mainly by their thermal, fluidic, and electrochemical behavior [2, 6, 10, 12]. If control strategies are to be designed for the two transient operating phases (heating and cooling) and for stationary operating points, it is essential to give special attention to the thermal subsystem. This subsystem corresponds to the most dominant system part during the control design for this type of application. This results from the fact that the admissibility of a control strategy for an SOFC system is usually defined by limitations on both

- the maximum fuel cell temperature and
- the admissible spatial and temporal variation rates of the internal stack temperature distribution [17].

The corresponding constraints have to be fulfilled to minimize mechanical strain due to different thermal expansion coefficients of the stack materials and, thus, to minimize degradation phenomena of the cell materials leading to prohibitively high operating costs. Due to the high complexity of fuel cell systems from a process engineering point of view and due to non-negligible nonlinearities and uncertainties, most state-of-the-art control strategies for SOFC systems are limited to constant or slowly varying operating conditions [18, 19]. However, such restrictions reduce the flexibility for using SOFC systems in a decentralized power grid, where transient operating conditions — caused by variations of the electrical load demand — are the usual case.

After a discretization of distributed parameter systems by employing the principle of an *early lumping approach* [20], control-oriented system models can be derived for the thermal behavior of SOFC systems which are given by nonlinear ordinary differential equations (ODEs). As shown in [12, 13], these ODEs can be derived by means of the first law of thermodynamics for non-stationary processes after a spatial semi-discretization of the fuel cell stack module. In this case, integral balance equations are derived which account for the inflow and outflow of energy into the selected finite volume elements. This balancing scheme leads to a model for the variation of the internal energy in each finite volume element. Since the variation of the internal energy are linked directly to the temperature variation in the corresponding element, it produces a set of nonlinear ODEs. These ODEs, firstly, describe the non-stationary behavior during the heating phase, secondly, the influence of variable electrical loads during usual system operation, and, finally, the non-stationary cooling process during the shutdown phase of the system.

The above-mentioned dynamic system model is characterized by a variety of physically motivated parameters which are linked to such effects as temperature-dependent specific heat capacities of the gases taking part in the electrochemical reaction, heat conduction and heat convection coefficients, and temperature-dependent reaction enthalpies. These parameters have been identified both by means of interval-based procedures and by means of floating point-based non-verified techniques. A detailed overview of the corresponding procedures and an extended description of the mathematical modeling procedures can be found in [1, 3, 12–14]. In the following, the interval-based parameter estimates determined in [1, 3, 13] serve as the starting point for the design of robust control laws. To obtain such controllers, we use an extension of classical sliding mode control [22, 23] making use of a suitable Lyapunov function to stabilize the system dynamics. Here, guaranteed stabilizing control laws are determined by a real-time application of interval arithmetic techniques. In such a way, a control

synthesis becomes possible which stabilizes the system dynamics, despite bounded uncertainty in the system parameterization and a-priori unknown disturbances. A first simulation study, published in [4], was carried out with the corresponding, guaranteed stabilizing enthalpy flow of the cathode gas as the control input.

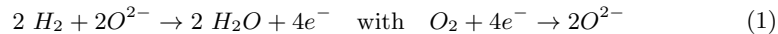
In this contribution, we extend our considerations in such a way that the enthalpy flow of the cathode gas into the stack module has to be controlled in an underlying procedure. This procedure manipulates both the air mass flow and the temperature difference between the supplied air in the preheating unit and the temperature inlet gas manifold of the fuel cell stack module. A real-time implementation of this underlying controller is presented in the current paper making use of an online optimization of a performance criterion which exploits a suitable interval multisection scheme. Coupling this multisection scheme with the above-mentioned sliding mode controller leads to determining the stabilizing enthalpy flow under consideration of further physical restrictions. These restrictions result from the admissible operating ranges of the air mass flow controller as well as from the temperature ranges that can be generated with the preheating unit installed in the test rig at the Chair of Mechatronics at the University of Rostock. Moreover, limitations for the temporal variation rates of the temperature difference between the preheating unit and the stack module's inlet gas manifold as well as for the variation of the cathode gas mass flow can be accounted for in this procedure. Both variation rates have to be taken into consideration to prevent damages due to thermal stress and actuator wear.

In Sec. 2, basic steps to derive control-oriented models for the thermal behavior of SOFC systems are briefly summarized. These models are analyzed in Sec. 3 with respect to their specific structure. Based on this structural analysis, feedback linearizing control strategies and novel interval-based sliding mode control procedures are derived. A numerical validation of these procedures is finally presented. Sec. 4 deals with the experimental validation of the control procedure on a real-life test rig, including a real-time capable disturbance observer and an online multisection scheme for the implementation of the underlying mass flow and temperature control of the cathode gas. Conclusions and an outlook on future work are presented in Sec. 5.

2 Modeling of the Thermal Behavior of SOFCs

A suitable nonlinear model for the description of the thermal behavior of SOFC systems in non-stationary operation is obtained from an integral formulation of the first law of thermodynamics. This formulation expresses the non-stationarity by means of variations of the internal energy of a stack module. These variations are also linked to variations of the internal temperature, which mainly depend on the enthalpy flows of both the supplied fuel gas and air as well as on heat conduction between the stacked fuel cell elements which are electrically connected in series.

If the overall exothermic chemical reaction



in a fuel cell element is enabled via an external electric current, leading to ion conduction in the interior of the stack module, the SOFC temperature additionally depends on the Ohmic loss characteristics of the fuel cell material as well as on the reaction enthalpy which is strongly affected by the choice of the fuel gas. In this paper, hydrogen (H_2) is used as a fuel gas in a mixture with nitrogen (N_2) and water vapor (H_2O).

Future work will also focus on gas mixtures containing methane, carbon-monoxide, and carbon-dioxide to emulate internal steam reforming processes on the test rig.

As a fundamental model, the thermal behavior can be described by a global energy balance. This type of model leads to a scalar ODE for the SOFC stack temperature. However, it is not capable of representing temperature gradients in the interior of an SOFC stack module with respect to the space coordinates. Such variations are specifically of interest if control strategies are designed for non-stationary operating phases such as heating and cooling. This restriction can be removed by a spatial semi-discretization of the temperature distribution, leading to a set of coupled ODEs for the complete stack module. A detailed derivation of such models can be found in [3, 12, 13] and the references therein. Disturbances and approximation errors caused by the finite-dimensional approximation of the original distributed parameter system can be quantified by observer techniques similar to those published in [11].

2.1 Global Energy Balances for the Thermal Behavior of SOFC Stacks

A first modeling approach for the temperature ϑ_{FC} in an SOFC stack module is based on the introduction of a single control volume. The energy flows passing the system boundary lead to variations of the internal energy in the corresponding volume element. This element is defined in such a way that the thermal insulation of the SOFC stack is contained in the interior of the system boundary according to Fig. 1.

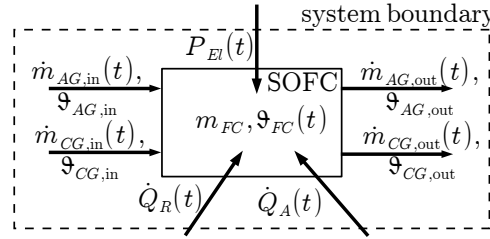


Figure 1: Global energy balance for a fuel cell module (AG: anode gas; CG: cathode gas; FC: fuel cell).

Here, the variation \dot{E}_{FC} of the internal energy is given by

$$\begin{aligned} \dot{E}_{FC}(t) = & C_{AG}(\vartheta_{FC}, t) \cdot (\vartheta_{AG,in}(t) - \vartheta_{AG,out}(t)) \\ & + C_{CG}(\vartheta_{FC}, t) \cdot (\vartheta_{CG,in}(t) - \vartheta_{CG,out}(t)) + \dot{Q}_R(t) + P_{El}(t) + \dot{Q}_A(t) , \end{aligned} \quad (2)$$

where $\vartheta_{FC} = \vartheta_{AG,out} = \vartheta_{CG,out}$ is commonly assumed. Additionally, the preheater temperatures ϑ_{AG} and ϑ_{CG} are assumed to be identical to the corresponding inlet gas manifold temperatures $\vartheta_{AG,in}$ and $\vartheta_{CG,in}$ in the stack module. Continuity of the mass flow finally leads to $\dot{m}_{AG,in} = \dot{m}_{AG,out} = \dot{m}_{AG}$ and $\dot{m}_{CG,in} = \dot{m}_{CG,out} = \dot{m}_{CG}$.

The heat flow \dot{Q}_A through the thermal insulation of the stack module is described by

$$\dot{Q}_A(t) = \frac{1}{R_{th,A}} \left(\vartheta_A - \vartheta_{FC}(t) \right) \quad (3)$$

with the thermal resistance $R_{th,A}$ of the insulation and the ambient temperature ϑ_A . To simplify the mathematical model, heat radiation is included in this expression in a

locally linearized form. This usually leads to (small) modeling errors in the case of high stack temperatures. To account for these errors and for non-negligible disturbances, an observer approach is presented in Sec. 3.6 that is capable of estimating the deviations between the model and the actual system behavior in real time. Additionally, the parameter identification of the control-oriented model accounts for the corresponding uncertainty by describing the coefficient $R_{th,A}$ as an interval.

The impact of the electrochemical processes, taking place in the interior of the stack module, is determined by $P_{El}(t) = R_{El} \cdot I(t)^2$. This heat flow represents the Ohmic losses resulting from the conduction of charge carriers in the fuel cell.

Moreover, the reaction heat flow

$$\dot{Q}_R(t) = \Delta_R H(\vartheta_{FC}) \cdot \dot{n}_{el}(t) = \Delta_R H(\vartheta_{FC}) \frac{I(t)}{z \cdot F}, \quad \dot{n}_{el}(t) = \frac{\dot{m}_{H_2}^R(t)}{M_{H_2}} \quad (4)$$

with the mass flow of hydrogen $\dot{m}_{H_2}^R$ (consumed in the electrochemical reaction), its molar mass M_{H_2} as well as the electrical current $I(t)$ is taken into account. The processes in (1) and (4) become relevant when connecting an electrical load to the SOFC stack module, where the maximum electrical current $I(t)$ between the electrodes is restricted by the consumed amount of hydrogen $\dot{m}_{H_2}^R$. This behavior is expressed by Faraday's law $I = z \cdot F \cdot \dot{n}_{el}$ for electrochemical reactions with the Faraday constant F as well as the number of electrons z which participate in each reaction (1).

The enthalpy flow in equation (2) contains the heat capacity of the anode gas mixture according to

$$C_{AG}(\vartheta_{FC}, t) = c_{H_2}(\vartheta_{FC}) \cdot \dot{m}_{H_2}(t) + c_{N_2}(\vartheta_{FC}) \cdot \dot{m}_{N_2}(t) + c_{H_2O}(\vartheta_{FC}) \cdot \dot{m}_{H_2O}(t), \quad (5)$$

where $\dot{m}_{H_2} \geq \dot{m}_{H_2}^R$ is the hydrogen mass flow that is supplied at the anode.

The corresponding heat capacity for the cathode gas is given by

$$C_{CG}(\vartheta_{FC}, t) = c_{CG}(\vartheta_{FC}) \cdot \dot{m}_{CG}(t) \quad (6)$$

with the mass flow $\dot{m}_{CG}(t)$ of air and its specific heat capacity $c_{CG}(\vartheta_{FC})$. The specific heat capacities of hydrogen $c_{H_2}(\vartheta_{FC})$, nitrogen $c_{N_2}(\vartheta_{FC})$, water vapor $c_{H_2O}(\vartheta_{FC})$ and air $c_{CG}(\vartheta_{FC})$ are approximated by second-order polynomials

$$c_\chi(\vartheta_{FC}) = \sum_{i=0}^2 \alpha_{\chi,i} \cdot \vartheta_{FC}^i. \quad (7)$$

The index $\chi \in \{H_2, N_2, H_2O, CG\}$ refers to each gas fraction. The fuel gas and the air mass flow \dot{m}_{CG} are preheated separately before they are supplied to the SOFC stack.

In analogy to (7), the reaction enthalpy $\Delta_R H(\vartheta_{FC})$ is approximated by a second-order polynomial. All parameters of this system model can be identified experimentally, see e.g., the work summarized in [3, 12, 14].

Finally, the variation of the internal energy $\dot{E}_{FC}(t)$ has to be related to the fuel cell temperature ϑ_{FC} by

$$\dot{\vartheta}_{FC}(t) = \frac{1}{c_{FC} \cdot m_{FC}} \dot{E}_{FC}(t). \quad (8)$$

In this equation, the specific heat capacity c_{FC} and the mass m_{FC} characterize averaged material parameters of the stack module which are assumed to be constant for the complete operating range. In the following, the equation (8) is abbreviated by the

scalar nonlinear ODE $\dot{\vartheta}_{FC}(t) = f(\vartheta_{FC}(t), \mathbf{p}, v(t))$ with the parameter vector \mathbf{p} and the enthalpy flow of the cathode gas $v = \dot{m}_{CG} \cdot (\vartheta_{CG} - \vartheta_{FC})$ as the control input. Note that bold variables are used throughout this paper to distinguish vectors from scalar variables. Interval variables are always denoted by square brackets.

2.2 Spatial Semi-Discretization of the Stack Module

As an extension to this basic model, the temperature distribution in the interior of the stack module can be described more accurately after a spatial semi-discretization.

For this purpose, the fuel cell stack is firstly divided into $L \cdot M \cdot N$ cuboids, where L , M and N represent the numbers of finite volume elements along each space coordinate which can be chosen in a problem-oriented way, see Fig. 2.

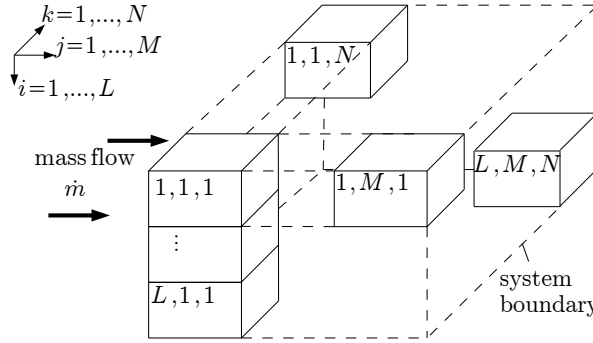


Figure 2: Spatial semi-discretization of the fuel cell stack module.

For each resulting volume element (i, j, k) , an integral energy balance

$$\begin{aligned} c_{i,j,k} m_{i,j,k} \dot{\vartheta}_{i,j,k}(t) &= C_{AG,i,j,k}(\vartheta, t) \cdot (\vartheta_{i,j-1,k}(t) - \vartheta_{i,j,k}(t)) \\ &+ C_{CG,i,j,k}(\vartheta, t) \cdot (\vartheta_{i,j-1,k}(t) - \vartheta_{i,j,k}(t)) \\ &+ \dot{Q}_{\eta,i,j,k}(t) + \dot{Q}_{R,i,j,k}(t) + P_{El,i,j,k}(t) \end{aligned} \quad (9)$$

is derived. Here, the local specific heat capacity $c_{i,j,k}$ and the local mass parameter $m_{i,j,k}$ serve as a replacement for the values c_{FC} and m_{FC} , respectively.

If the inter-element conditions derived in [13, 15] which characterize the continuity of the heat flow over each boundary surface between neighboring finite volume elements are included additionally, a set of ODEs

$$\dot{\mathbf{x}}(t) = \mathbf{f}(\mathbf{x}(t), \mathbf{p}, \mathbf{u}(t)) \quad (10)$$

is obtained with the states $\mathbf{x}^T = (\vartheta_{1,1,1} \dots \vartheta_{L,M,N}) \in \mathbb{R}^{n_x}$. Also in this case, the parameters \mathbf{p} have to be identified experimentally as for the global energy balance described in the previous section.

For both the global system model and the semi-discretized one, the control vector $\mathbf{u}(t)$ consists of the mass flow $\dot{m}_{CG,in}(t)$ of preheated cathode gas with the temperature difference $\Delta\vartheta(t) := \vartheta_{CG,in}(t) - \vartheta_{FC,in}(t)$, where $\vartheta_{CG,in}(t)$ is the cathode gas temperature of the inlet manifold, and $\vartheta_{FC,in}(t)$ is the temperature of the stack module's inlet gas manifold itself.

Further modifications — necessary to determine the system model with improved spatial resolution — are the following. Firstly, the term

$$\dot{Q}_{\eta,i,j,k}(t) = \sum_{\eta \in \mathcal{N}} \frac{1}{R_{th,\eta}^{i,j,k}} (\vartheta_{\eta}(t) - \vartheta_{i,j,k}(t)) \quad (11)$$

has to be introduced to characterize the heat transfer and the heat conduction by the thermal resistance $R_{th,\eta}^{i,j,k}$ from all neighboring volume elements denoted by the multi index $\eta \in \mathcal{N}$, $\mathcal{N} = \{(i-1, j, k), (i+1, j, k), (i, j-1, k), (i, j+1, k), (i, j, k-1), (i, j, k+1)\}$, to the volume element (i, j, k) . With this notation, the following boundary conditions hold: $\vartheta_{i-1,j,k} = \vartheta_A$ for $i = 1$ and $\vartheta_{i+1,j,k} = \vartheta_A$ for $i = L$, $\vartheta_{i,j-1,k} = \vartheta_P$ for $j = 1$, $\vartheta_{i,j+1,k} = \vartheta_A$ for $j = M$, $\vartheta_{i,j,k-1} = \vartheta_A$ for $k = 1$ and $\vartheta_{i,j,k+1} = \vartheta_A$ for $k = L$, where ϑ_P is the temperature of the preheated supply gases.

In the global energy balance, only a special case of the term (11) is included, namely, the heat transfer from the fuel cell stack to the ambient medium. For the semi-discretized version, it also accounts for heat conduction in the interior of the stack module, where the thermal resistances between neighboring interior elements have to be distinguished from those located at the system boundary.

Secondly, the reaction enthalpy has to be replaced by a local representation

$$\dot{Q}_{R,i,j,k}(t) = \frac{\Delta_R H_{i,j,k}(\vartheta_{i,j,k}) \cdot \dot{m}_{H_2,i,j,k}^R(t)}{M_{H_2}}, \quad (12)$$

with the corresponding temperature-dependent molar reaction enthalpy $\Delta_R H_{i,j,k}(\vartheta_{i,j,k})$ and the local molar flow of hydrogen $\frac{\dot{m}_{H_2,i,j,k}^R}{M_{H_2}}$. As before, Faraday's law for electrochemical reactions yields

$$\dot{Q}_{R,i,j,k}(t) = \Delta_R H_{i,j,k}(\vartheta_{i,j,k}) \frac{I_{i,j,k}(t)}{z \cdot F} \quad (13)$$

with the electric current $I_{i,j,k}$ in the corresponding volume element, the Faraday constant F and the number of electrons z transferred in the reaction (1) [2].

Thirdly, also the electric current $I_{i,j,k}$ has to be substituted by its local representation, leading to the Ohmic loss characteristics $P_{El,i,j,k}(t) = R_{El,i,j,k} I_{i,j,k}^2(t)$ with the internal resistance $R_{El,i,j,k}$. For the computation of the heat capacities $C_{AG,i,j,k}(\vartheta_{i,j,k}, t)$ and $C_{CG,i,j,k}(\vartheta_{i,j,k}, t)$ of the fluids inside each finite volume element, the local consumption of hydrogen H_2 at the anode, oxygen O_2 at the cathode and the local production of water vapor H_2O at the anode have to be taken into account as described in [13] as a generalization of the model in Subsection 2.1.

In the following, control procedures are derived for configuration *I*, corresponding to the global energy balance, and for configuration *II*. The following structural analysis also touches upon extensions that will become necessary if a spatial discretization is performed in two or three coordinates, e.g., for configuration *III* in Fig. 3.

3 Structural Analysis and Control Design

In this section, the system models summarized in Fig. 3 are analyzed with respect to the structural properties which are relevant for a design of observer-based robust control strategies.

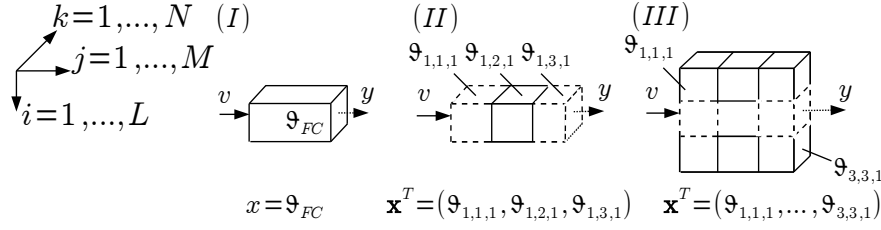


Figure 3: Different variants of the semi-discretization of the fuel cell stack module.

3.1 Structural Analysis of the Global SOFC Model

To design a robust sliding mode control strategy, the SOFC model has to be rewritten into an input-affine system representation. This form can be obtained directly as

$$\begin{aligned} \dot{\vartheta}_{FC} &= f(\vartheta_{FC}(t), \mathbf{p}, d, v(t)) = a(\vartheta_{FC}(t), \mathbf{p}) + d + \tilde{b}(\vartheta_{FC}(t), \mathbf{p}) \cdot v(t) \\ &= \tilde{a}(\vartheta_{FC}(t), \mathbf{p}, d) + \tilde{b}(\vartheta_{FC}(t), \mathbf{p}) \cdot v(t) \end{aligned} \quad (14)$$

with the interval parameter vector $\mathbf{p} \in [\mathbf{p}] = [\underline{\mathbf{p}}; \overline{\mathbf{p}}]$ and the disturbance $d \in [d] = [\underline{d}; \overline{d}]$ if a scalar system representation (configuration I) is taken into consideration. In the definition of the uncertain quantities, $\underline{\mathbf{p}} \leq \overline{\mathbf{p}}$ and $\underline{d} \leq \overline{d}$ hold component-wise.

In (14), the term \tilde{b} is chosen in such a way that strict positivity $\tilde{b}(\vartheta_{FC}(t), \mathbf{p}, d) > 0$ is guaranteed despite uncertainties in \mathbf{p} and d . Then, the terms $a(\vartheta_{FC}(t), \mathbf{p})$ and $\tilde{b}(\vartheta_{FC}(t), \mathbf{p})$ in (14) can be expressed by

$$\begin{aligned} a(\vartheta_{FC}, \mathbf{p}) &= \frac{C_{AG}(\vartheta_{FC}, t)(\vartheta_{AG}(t) - \vartheta_{FC}(t))}{c_{FC} m_{FC}} + \frac{(\vartheta_A - \vartheta_{FC})}{c_{FC} m_{FC} R_{th,A}^{FC}} \\ &+ \frac{\Delta_R H}{c_{FC} m_{FC} z F} I + \frac{R_{El,FC}}{c_{FC} m_{FC}} I^2 \end{aligned} \quad (15)$$

and

$$\tilde{b}(\vartheta_{FC}, \mathbf{p}) = \frac{c_{CG}}{c_{FC} m_{FC}}, \quad (16)$$

respectively. The additive disturbance $d \in [d]$ in (14) is estimated in real time by a suitable observer.

Moreover, the system input $v(t)$ represents the cathode gas enthalpy flow

$$v(t) = \dot{m}_{CG}(t) \cdot (\vartheta_{CG}(t) - \vartheta_{FC}(t)) . \quad (17)$$

3.2 Structural Analysis of the Semi-Discretized Model

The derivation of the input-affine system representation for the case II makes use of successive differentiations of the output equation $y = h(\mathbf{x})$ (corresponding to the temperature $\vartheta_{1,M,1}$ at the outlet gas manifold) with the Lie derivatives

$$y^{(i)} = L_f^i h(\mathbf{x}) = L_f (L_f^{i-1} h(\mathbf{x})), \quad i = 0, \dots, \delta - 1, \quad (18)$$

for which $y = h(\mathbf{x}) = L_f^0 h(\mathbf{x})$ holds for $i = 0$ with the relative degree $\delta = M$, see [8].

Assuming that the direct influence of $v(t)$ on the state variables $\vartheta_{1,2,1}, \dots, \vartheta_{1,M,1}$ due to variations of \dot{m}_{CG} is sufficiently small, the relation $\frac{\partial L_{\mathbf{f}}^i h(\mathbf{x})}{\partial v} = 0$ holds for all $i = 0, \dots, M - 1$.

Using the new state vector

$$\mathbf{z}^T = (h(\mathbf{x}) \quad L_{\mathbf{f}}h(\mathbf{x}) \quad \dots \quad L_{\mathbf{f}}^{M-1}h(\mathbf{x}))^T \in \mathbb{R}^M, \quad (19)$$

the state equations (10) of the case *II* can be transformed into the nonlinear state-space representation

$$\dot{\mathbf{z}} = \begin{pmatrix} L_{\mathbf{f}}h(\mathbf{x}) \\ \vdots \\ L_{\mathbf{f}}^{M-1}h(\mathbf{x}) \\ L_{\mathbf{f}}^M h(\mathbf{x}) \end{pmatrix} = \begin{pmatrix} z_2 \\ \vdots \\ z_M \\ \tilde{a}(\mathbf{z}, \mathbf{p}, d) \end{pmatrix} + \begin{pmatrix} 0 \\ \vdots \\ 0 \\ \tilde{b}(\mathbf{z}, \mathbf{p}) \end{pmatrix} \cdot v. \quad (20)$$

Here, the additive bounded disturbance $d \in [d] = [\underline{d}; \bar{d}]$ and the interval parameters $\mathbf{p} \in [\mathbf{p}]$ are defined as for the scalar case (*I*). Moreover, the relations

$$\tilde{a}(\mathbf{z}, \mathbf{p}, d) = L_{\mathbf{f}}^M h(\mathbf{x}) - \tilde{b}(\mathbf{z}, \mathbf{p}) \cdot v + d, \quad (21)$$

and

$$\tilde{b}(\mathbf{z}, \mathbf{p}) = \frac{\partial L_{\mathbf{f}}^M h(\mathbf{x})}{\partial v} > 0 \quad (22)$$

hold, where the last inequality is true for all possible operating points of the fuel cell system due to physical conditions for the signs of the parameters contained in the vector \mathbf{p} .

This guarantees that the state $\vartheta_{1,M,1}$ is the flat system output. Hence, a design of flatness-based and feedback linearizing controllers becomes possible. For the case of generalizations to the control of non-flat outputs, the reader is referred to the basic remarks given in [15]. An experimental validation of corresponding controllers is the subject of ongoing research activities. If a semi-discretization is performed in at least two space coordinates (configuration *III*), the temperature at a specific point in the outlet gas manifold is usually no longer the flat system output. Then, $\delta < n_x$ holds in (18)–(20). In this case, all state variables, which cannot be parameterized according to (20), have to be treated as bounded disturbances in the subsequent control design.

3.3 Feedback Linearizing Control Design

The nonlinear controller canonical form (20) can be stabilized asymptotically by

$$v := \frac{-\tilde{a}(\mathbf{z}, \mathbf{p}, d) + \nu}{\tilde{b}(\mathbf{z}, \mathbf{p})}, \quad (23)$$

which compensates the nonlinear system dynamics exactly and results in an integrator chain of length δ with the output $y = h(\mathbf{x}) = \vartheta_{1,M,1}$.

The asymptotic stabilization of this integrator chain can be achieved by the state feedback

$$\nu(t) = -\alpha_0 z_1 - \alpha_1 z_2 - \dots - \alpha_{M-1} z_M + \mu(t). \quad (24)$$

In (24), the parameters $\alpha_0, \alpha_1, \dots, \alpha_{M-1}$ have to be chosen as coefficients of a Hurwitz polynomial of the order $\delta = M$. Substituting the input ν defined in (24) for the corresponding term in (23) leads to the control signal

$$v := \frac{-\tilde{a}(\mathbf{z}, \mathbf{p}, d) - \alpha_0 h(\mathbf{x}) - \alpha_1 L_{\mathbf{f}} h(\mathbf{x}) - \dots - \alpha_{M-1} L_{\mathbf{f}}^{M-1} h(\mathbf{x}) + \mu(t)}{\tilde{b}(\mathbf{z}, \mathbf{p})} . \quad (25)$$

To guarantee steady-state accuracy for the desired temperature $\vartheta_{1,M,1,d}$, the feed-forward part of the control law has to be chosen as

$$\mu = \beta_0 \vartheta_{1,M,1,d} \quad \text{with} \quad \beta_0 = \alpha_0 . \quad (26)$$

Analogously, perfect tracking of desired temperature profiles (in case of exactly known parameters \mathbf{p} and disturbances d) can be obtained by $\beta_0 = \alpha_0, \beta_1 = \alpha_1, \dots, \beta_{M-1} = \alpha_{M-1}$ in the feedforward control law

$$\mu = \beta_0 \vartheta_{1,M,1,d} + \beta_1 \dot{\vartheta}_{1,M,1,d} + \dots + \beta_{M-1} \vartheta_{1,M,1,d}^{(M-1)} . \quad (27)$$

In Fig. 4(a), a complete heat-up process is shown for a simulation time of $T = 30,000$ s with a desired trajectory for the temperature $\vartheta_{1,M,1,d}$ and the number of elements $M = 3$.

This simulation shows a maximum tracking error of $|e| = 1.4\text{K}$, which mostly results from parameter uncertainties and from variations of the anode gas properties which are unknown to the controller (in the simulation all anode gas parameters are replaced by measured data from the test rig).

The output signal defined in (25) is depicted in Fig. 4(c). It represents the manipulation of the enthalpy flow of the cathode gas. Its negative value partially compensates a simultaneous constant heating by the enthalpy flow of the anode gas. To compensate non-modeled or a-priori unknown disturbances, the control law is extended by a variable structure component in the following subsection.

3.4 Robust Sliding Mode Control

To design an interval-based sliding mode controller, which guarantees asymptotic stability of the closed-loop control system during transient and stationary operating conditions despite interval parameters $[\mathbf{p}]$ and $[d]$, the tracking error of all components of \mathbf{z} is defined by the time derivatives

$$\tilde{z}_1^{(j)} = z_1^{(j)} - z_{1,d}^{(j)} \quad \text{with} \quad j = 0, \dots, \delta - 1 = M - 1 \quad (28)$$

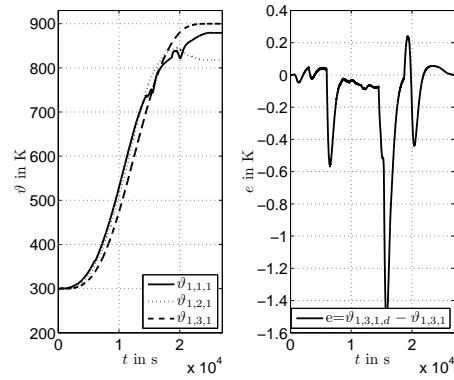
and the system output $\vartheta_{1,M,1} = z_1 = z_1^{(0)}$.

Perfect tracking of a given trajectory $z_{1,d}^{(j)}$ corresponds to state trajectories which are located on the sliding surface

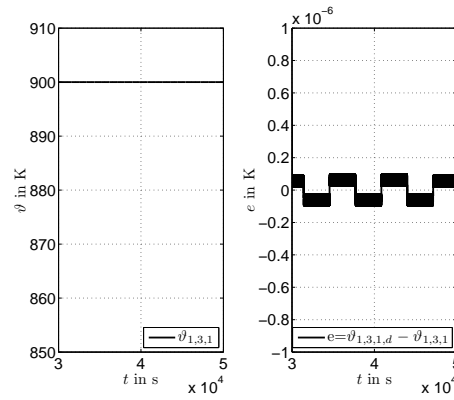
$$s(\tilde{\mathbf{z}}) = \tilde{z}_1^{(M-1)} + \alpha_{M-2} \tilde{z}_1^{(M-2)} + \dots + \alpha_0 \tilde{z}_1^{(0)} = 0 . \quad (29)$$

To guarantee asymptotic stability of the dynamics on this sliding surface, the parameters $\alpha_0, \dots, \alpha_{M-2}$ have to be chosen as coefficients of a Hurwitz polynomial of order $M - 1$. Moreover, the stabilization of \mathbf{z} towards the sliding surface can be achieved for $s \neq 0$ if a variable structure control law is defined on the basis of the Lyapunov function

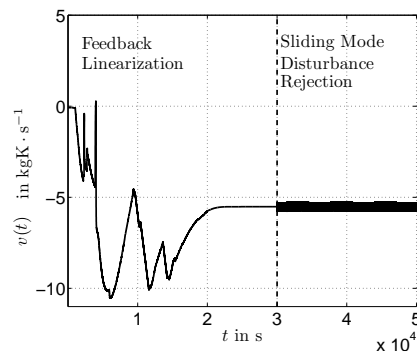
$$V = \frac{1}{2} s^2 > 0 \quad \text{for} \quad s \neq 0 . \quad (30)$$



(a) Tracking control of a non-stationary heating process according to (25).



(b) Sliding mode-based disturbance compensation for the desired operating point $\vartheta_{1,3,1,d} = \text{const.}$



(c) Controller output $v(t)$.

Figure 4: System outputs of the feedback linearizing controller (a), the interval-based sliding mode controller (b), and corresponding control signals (c).

For the derivation of this control law, the time derivative

$$\dot{V} = s\dot{s} \leq 0 \tag{31}$$

is replaced by the more strict requirement

$$\dot{V} = s\dot{s} \leq -\eta|s| = -\eta s \cdot \text{sign}\{s\} , \quad \eta > 0 . \tag{32}$$

In (32), the derivative of (29) is expressed in terms of the state equations (20) with the tracking errors (28). This leads to

$$\begin{aligned} \dot{s}(\tilde{\mathbf{z}}) &= \dot{z}_1^{(M)} + \alpha_{M-2}\dot{z}_1^{(M-1)} + \dots + \alpha_0\dot{z}_1^{(1)} \\ &= \tilde{a}(\mathbf{z}, \mathbf{p}, d) + \tilde{b}(\mathbf{z}, \mathbf{p}) \cdot v - z_{1,d}^{(M)} + \alpha_{M-2}\dot{z}_1^{(M-1)} + \dots + \alpha_0\dot{z}_1^{(1)} . \end{aligned} \tag{33}$$

Furthermore, $s\dot{s} \leq -\eta \cdot s \cdot \text{sign}\{s\}$ can be reformulated as $s \cdot (\dot{s} + \eta \cdot \text{sign}\{s\}) \leq 0$. This is guaranteed by

$$\dot{s} + \eta \cdot \text{sign}\{s\} = -\beta \cdot \text{sign}\{s\} , \tag{34}$$

where $\eta, \beta > 0$ holds for both parameters.

Substituting \dot{s} defined by (33) for the corresponding term in (34) yields the control law

$$\begin{aligned} [v] := & \left[\frac{-\tilde{a}(\mathbf{z}, \mathbf{p}, d) + z_{1,d}^{(M)} - \alpha_{M-2}\dot{z}_1^{(M-1)} \dots - \alpha_0\dot{z}_1^{(1)}}{\tilde{b}(\mathbf{z}, \mathbf{p})} \right. \\ & \left. - \frac{1}{\tilde{b}(\mathbf{z}, \mathbf{p})} \underbrace{(\eta + \beta)}_{=: \tilde{\eta} > 0} \cdot \text{sign}\{s\} \right] \Bigg|_{\substack{\mathbf{p} \in [\mathbf{p}] \\ d \in [d]}} . \end{aligned} \tag{35}$$

During the interval-based evaluation of (35) by means of the toolbox C-XSC [7] in a real-time rapid control prototyping environment (a point-valued term d is estimated by the procedure described in Subsection 3.6), the following cases have to be distinguished for the controller output to guarantee asymptotic stability despite the uncertainties $[\mathbf{p}]$ and $[d]$:

$$v := \begin{cases} \bar{v} := \sup\{[v]\} & \text{for } s \geq 0 \\ \underline{v} := \inf\{[v]\} & \text{for } s < 0 . \end{cases} \tag{36}$$

Here, s is evaluated directly for measured data.

If this controller is designed for the scenario *II* with $M = 3$ and activated after the feedback linearizing controller finalized the heat-up phase of the SOFC system, the results in Fig. 4(b) and Fig. 4(c) can be obtained. Here, the guaranteed stabilization of the system and its robustness are achieved by an appropriate choice of $\tilde{\eta}$ in (35), leading to the negative definiteness of \dot{V} . In the simulation, the time-dependent disturbance $d := 1 \cdot 10^{-8} \text{sign}\{\sin(0.001t)\} \in [-1 ; 1] \cdot 10^{-8}$ was active between $t = 30,000\text{s}$ and $t = 50,000\text{s}$ with a fixed desired operating point $\vartheta_{1,3,1,d} = \text{const}$.

Since it is necessary to synthesize the cathode gas enthalpy flow by an underlying control of the corresponding mass flow and preheater temperature, the following online optimization procedure is employed.

3.5 Subdivision Strategy for the Real-Time Implementation of the Control Law

The remainder of this paper is restricted to the global model for the stack temperature. However, extensions to the semi-discretized system model can be made in a straightforward manner. A subdivision strategy is used to determine appropriate control inputs $\dot{m}_{CG}(t)$ and $\Delta\vartheta(t) := \vartheta_{CG}(t) - \vartheta_{FC}(t)$ corresponding to the interval-based control signal $[v(t)]$. The control vector of the SOFC system is defined as

$$\mathbf{u}(t) := \begin{pmatrix} \dot{m}_{CG}(t) \\ \Delta\vartheta(t) \end{pmatrix}. \quad (37)$$

Here, the product of both the mass flow $\dot{m}_{CG}(t)$ and the temperature difference $\Delta\vartheta(t)$ has to comply with (36). In addition, unnecessarily large temporal variations of the control signal between two subsequent time step in a discrete-time evaluation should be prevented. Moreover, it is essential to determine the control vector $\mathbf{u}(t)$ in such a way that it becomes efficient from an energy point of view.

These goals can be reached by the following subdivision strategy. In each point of time t_k , the following subdivision is initialized with the intervals $[\dot{m}_{CG}^{<0>}]$ and $[\Delta\vartheta^{<0>}]$, corresponding to the actuator constraints of the system. Now, a multi-section procedure for the corresponding interval vector $[\mathbf{u}^{<0>}]$ is started.

Interval vectors $[\mathbf{u}^{<l>}]$ fulfilling the conditions

$$v := \begin{cases} \sup\{[v]\} < \inf\{[\dot{m}_{CG}^{<l>}] \cdot [\Delta\vartheta^{<l>}]\} & \text{for } s(t) \geq 0 \\ \inf\{[v]\} > \sup\{[\dot{m}_{CG}^{<l>}] \cdot [\Delta\vartheta^{<l>}]\} & \text{for } s(t) < 0 \end{cases} \quad (38)$$

represent the sets of guaranteed admissible system inputs. These intervals are temporarily stored in a separate list of length L^* .

Inconsistent intervals

$$v := \begin{cases} \sup\{[v]\} > \sup\{[\dot{m}_{CG}^{<l>}] \cdot [\Delta\vartheta^{<l>}]\} & \text{for } s(t) \geq 0 \\ \inf\{[v]\} < \inf\{[\dot{m}_{CG}^{<l>}] \cdot [\Delta\vartheta^{<l>}]\} & \text{for } s(t) < 0 \end{cases} \quad (39)$$

are deleted. All remaining intervals $[\mathbf{u}^{<l>}]$ from a list of length L are further subdivided for a predefined number of times into four subboxes each. In this subdivision, the vectors

$$\begin{aligned} \begin{pmatrix} [\dot{m}_{CG}^{<l>}] \\ [\Delta\vartheta^{<l>}] \end{pmatrix} &:= \begin{pmatrix} [\inf([\dot{m}_{CG}^{<l>}]); \text{mid}([\dot{m}_{CG}^{<l>}])] \\ [\inf([\Delta\vartheta^{<l>}]); \text{mid}([\Delta\vartheta^{<l>}])] \end{pmatrix}, \\ \begin{pmatrix} [\dot{m}_{CG}^{<L+1>}] \\ [\Delta\vartheta^{<L+1>}] \end{pmatrix} &:= \begin{pmatrix} [\text{mid}([\dot{m}_{CG}^{<l>}]); \text{sup}([\dot{m}_{CG}^{<l>}])] \\ [\inf([\Delta\vartheta^{<l>}]); \text{mid}([\Delta\vartheta^{<l>}])] \end{pmatrix}, \\ \begin{pmatrix} [\dot{m}_{CG}^{<L+2>}] \\ [\Delta\vartheta^{<L+2>}] \end{pmatrix} &:= \begin{pmatrix} [\inf([\dot{m}_{CG}^{<l>}]); \text{mid}([\dot{m}_{CG}^{<l>}])] \\ [\text{mid}([\Delta\vartheta^{<l>}]); \text{sup}([\Delta\vartheta^{<l>}])] \end{pmatrix} \text{ and} \\ \begin{pmatrix} [\dot{m}_{CG}^{<L+3>}] \\ [\Delta\vartheta^{<L+3>}] \end{pmatrix} &:= \begin{pmatrix} [\text{mid}([\dot{m}_{CG}^{<l>}]); \text{sup}([\dot{m}_{CG}^{<l>}])] \\ [\text{mid}([\Delta\vartheta^{<l>}]); \text{sup}([\Delta\vartheta^{<l>}])] \end{pmatrix}. \end{aligned} \quad (40)$$

are obtained. All of them are again checked for admissibility. Guaranteed admissible control intervals are shifted to the list of length L^* , all inadmissible ones are deleted,

and all intervals for which the admissibility cannot be decided on are kept in the list of length L .

The optimal control input is now chosen from the list of guaranteed admissible inputs by an online evaluation of the performance criterion

$$\begin{aligned}
 [J_k^{<l>}] = & \kappa_1 \cdot ([\Delta\vartheta_k^{<l>}])^2 + \kappa_2 \cdot ([\dot{m}_{CG,k}^{<l>}])^2 + \\
 & \kappa_3 \cdot ([\Delta\vartheta_k^{<l>}] - [\Delta\vartheta_{k-1}])^2 + \kappa_4 \cdot ([\dot{m}_{CG,k}^{<l>}] - [\dot{m}_{CG,k-1}])^2 .
 \end{aligned} \tag{41}$$

according to

$$l^* = \arg \min_{l=1, \dots, L^*} \{ \inf [J_k^{<l>}] \} \tag{42}$$

leading to an optimized control vector

$$\mathbf{u} := \begin{pmatrix} \text{mid}[\dot{m}_{CG,k}^{<l^*>}] \\ \text{mid}[\Delta\vartheta^{<l^*>}] \end{pmatrix} \tag{43}$$

that guarantees asymptotic stability of the closed-loop control system. In (41), the factors κ_1 and κ_2 have to be chosen such that the control procedure becomes energy-efficient, while the terms κ_3 and κ_4 aim at the prevention of unnecessarily large variations of the actual control signals.

An illustration of the admissibility test that was described above is shown in Fig. 5 for $s > 0$. In this figure, the actuator constraints are depicted by dotted lines. On the left-hand side, the test described above is shown in the $([\dot{m}_{CG}], [\Delta\vartheta])$ -plane in which the guaranteed admissible interval boxes have to be detected. The right-hand side visualizes the corresponding backward transformation into the virtual control input v as a function of time t .

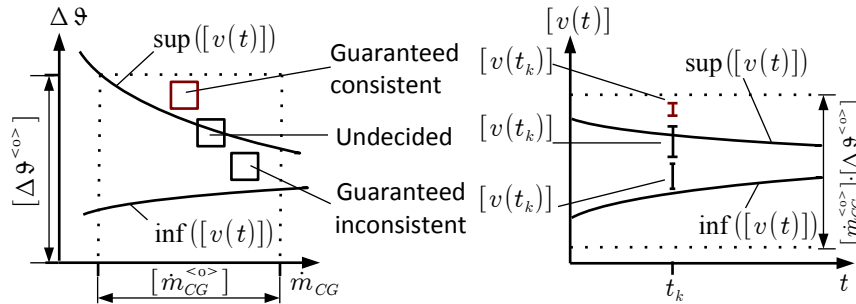


Figure 5: Subdivision strategy for the point of time $t = t_k$.

Additionally, Fig. 6 shows the maximum admissible control errors (restricted to a region of ± 50 K around the desired temperature profile) that can be stabilized by means of this procedure under consideration of the actuator constraints $[\mathbf{u}^{<0>}]$ for different control parameters $\tilde{\eta}$ and different disturbance intervals $[d]$. The numerical evaluation has been performed for the anode gas inputs and for the reference trajectory (white curve) that are also used in the experimental validation presented in the following section (see Figs. 8 and 9). From Fig. 6, it becomes obvious that decreasing the parameter $\tilde{\eta} > 0$ typically leads to larger regions (dark gray) which can be stabilized with certainty under consideration of the actuator constraints defined in Fig. 5.

Middle gray domains are undecided since the control signal lies partially inside and partially outside the domain in Fig. 5 if the interval control law $[v]$ is evaluated. All light gray regions cannot be proven to contain stabilizable operating points for a fixed value $\tilde{\eta}$. However, this decrease of $\tilde{\eta}$ typically goes along with a reduced convergence rate to the desired temperature profile. Therefore, future work also will have to deal with an online adaptation of $\tilde{\eta}$ and with a reduction of the interval widths of $[d]$ by means of advanced estimation procedures. Both approaches seem to be promising since there exist cases in which an increase of $\tilde{\eta}$ leads to shifting the domains that are guaranteed to be stabilizable towards later points of time with higher operating temperatures.

3.6 Observer-Based Control Strategy

To avoid control parameterizations which lead to unacceptably slow dynamics due to excessively conservative a-priori estimates for parameters and disturbances, it is essential to apply techniques that are capable of estimating model errors during the operation of the plant in real time. This goal can be reached by the design of a combined state and disturbance observer reconstructing both model errors resulting from the simplifications made in Sec. 2.1 and external disturbances on the basis of the measured stack temperature $\vartheta_{FC}(t_k)$. The interfaces of this observer with the test rig and the interval-based control procedure are visualized in Fig. 7.

For the system configuration I , the values estimated by the observer correspond to the stack temperature $\hat{\vartheta}_{FC}$ and the disturbance \hat{d} . Hence, the corresponding observer ODE can be obtained as an extension of the thermal subsystem, given in (14) with (15) and (16), according to

$$\frac{d}{dt} \begin{pmatrix} \hat{\vartheta}_{FC} \\ \hat{d} \end{pmatrix} = \begin{pmatrix} \tilde{a}(\hat{\vartheta}_{FC}, \mathbf{p}, \hat{d}) + \tilde{b}(\hat{\vartheta}_{FC}, \mathbf{p}) \cdot v \\ 0 \end{pmatrix} + \begin{pmatrix} h_1 \\ h_2 \end{pmatrix} \cdot \Delta y . \quad (44)$$

In (44), the term $\Delta y = (\vartheta_{FC,m} - \hat{\vartheta}_{FC})$ characterizes the deviation between the measured stack temperature $\vartheta_{FC,m}$ and its estimate $\hat{\vartheta}_{FC}$. Note that the observer gains h_1 and h_2 have to be determined in such a way that the error dynamics of the observer (44) is stabilized asymptotically. This can be achieved by means of pole placement for the observer error dynamics after a linearization of the nonlinear ODE (14) for the state estimate $(\hat{\vartheta}_{FC} \quad \hat{d})^T$.

In Fig. 7, the estimates that are determined by this observer are fed back into the interval-based control law (35). Here, the estimated temperature $\hat{\vartheta}_{FC}$ serves as a low-pass filtered substitute for the measured data. Moreover, the a-priori estimates on the interval bounds for the disturbance d can now be replaced by a time-varying enclosure $[d(t)] = [\underline{d}(t); \bar{d}(t)]$ with the lower bound $\underline{d}(t) = \hat{d}(t) - \Delta d$ and the upper bound $\bar{d}(t) = \hat{d}(t) + \Delta d$. Here, the parameter $\Delta d > 0$ must be determined empirically from measured data. Finally, it is assumed that the anode gas mass flow \dot{m}_{AG} and its temperature ϑ_{AG} are controlled over the complete operation by a suitable structure that is independent of the cathode gas controller. However, the cathode gas control strategy receives corresponding measured data for \dot{m}_{AG} and ϑ_{AG} as additional input signals.

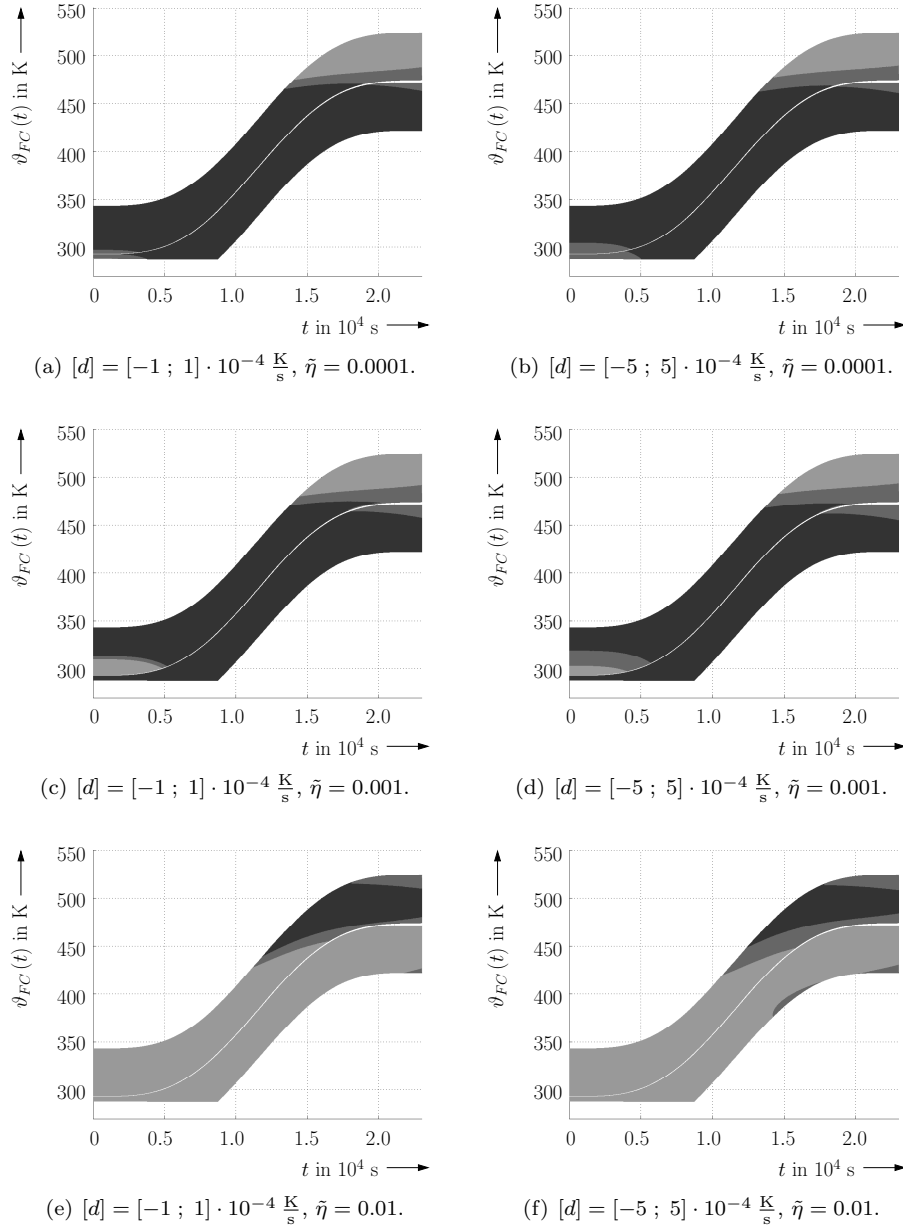


Figure 6: Guaranteed stabilizable control errors for each point of time t with different disturbance intervals $[d]$ and different controller parameters $\tilde{\eta}$ (dark gray: guaranteed stabilizable; middle gray: undecided; light gray: control exceeds actuator constraints).

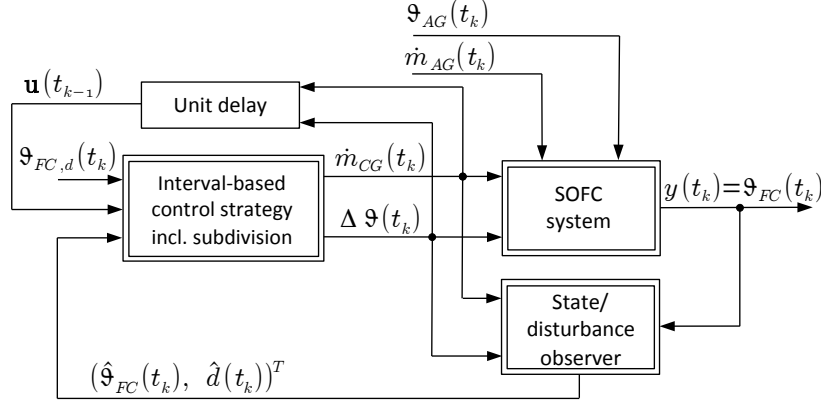


Figure 7: Disturbance observer for the estimation of the modeling errors and for the improvement of the control performance.

4 Experimental Validation of the Interval-Based Sliding Mode Controller

The observer-based control law, derived in the previous section, has been implemented as a C++ code using the library C-XSC [7] to provide functionalities for basic interval computations [5]. This controller includes the subdivision strategy for the online optimization of the system inputs. It has been interfaced with the rapid control prototyping environment cRIO provided by National Instruments which is used for the open-loop and closed-loop control of the available SOFC test rig. Here, an interface routine is implemented between the C++ code of the controller (included in a Simulink s-function) and LABVIEW by using the *Simulation Interface Toolkit* [9, 21]. In this section, experimental results are presented for the observer-based control strategies described above.

As shown in Fig. 7, underlying commercial feedforward controllers are used in this experiment to provide the anode gas mass flow by means of the available mass flow controller with its corresponding preheater temperature to the inlet gas manifold of the SOFC stack module. The corresponding values are measured in real time and passed on to the system model that is included in the interval-based sliding mode control strategy. This controller computes piecewise constant approximations for the enthalpy flow of the cathode gas with a sampling time of 0.5 s. This enthalpy flow, characterized by the interval variable $[v]$, is later split into the optimized mass flow \dot{m}_{CG} and the preheater temperature $\vartheta_{CG} = \vartheta_{FC} + \Delta\vartheta$. This optimization is performed in real time according to the criterion (41) in each sampling step.

The goal of the following experiment is the validation of the implemented controller for heating up the stack module from the initial temperature $\vartheta_{FC} = 297.0\text{K}$ up to its final value of $\vartheta_{FC} = 473.0\text{K}$ in the time horizon $T_{exp} = 23,000\text{s}$.

Fig. 8(a) shows the preheater temperatures for both the anode gas (dashed line) and the cathode gas (solid line). The corresponding constant anode gas mass flow \dot{m}_{AG} (consisting of nitrogen N_2 , dashed line) and the cathode gas mass flow \dot{m}_{CG} (solid line) are depicted in Fig. 8(b).

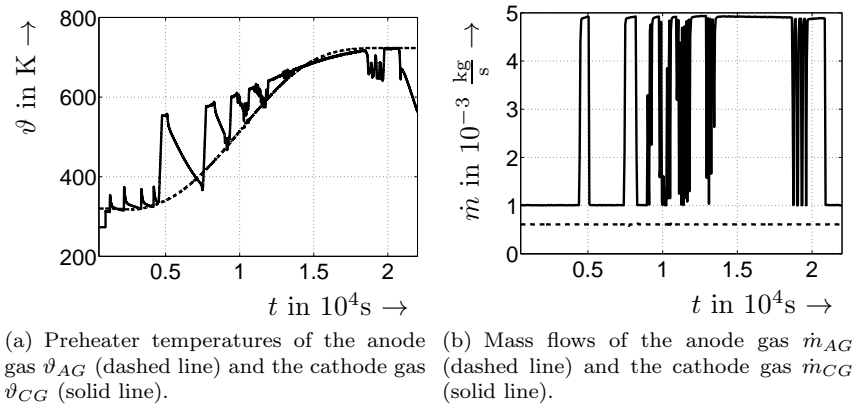


Figure 8: System inputs of the stack module during the heat-up phase.

In Fig. 9(a), the desired trajectory $\vartheta_{FC,d}$ (parameterized in an analytic form as a continuously differentiable polynomial) and the measured stack temperature $\vartheta_{FC,m}$ are compared. The resulting error signal $e = \vartheta_{FC,d} - \vartheta_{FC,m}$ describes the deviation between these values as shown in Fig. 9(b). The combination of the interval-based sliding mode controller with the model-based state and disturbance observer leads to an excellent tracking of the desired trajectory even in the transient phase.

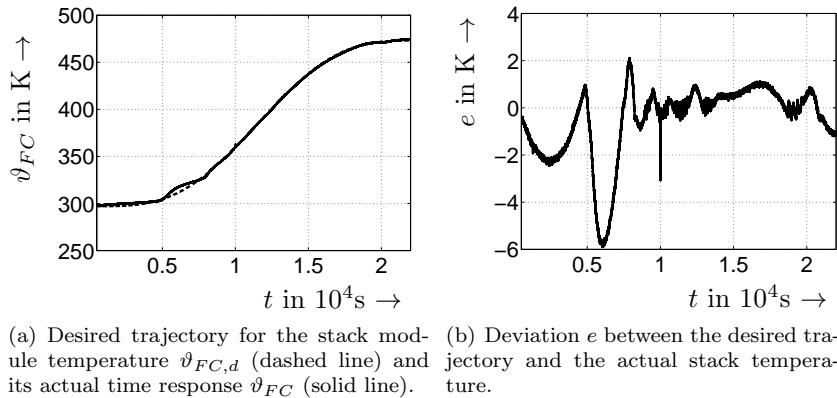


Figure 9: Experimental results of the disturbance observer-based interval sliding mode control procedure.

The outputs of the combined state and disturbance observer (44) are shown in Fig. 10. The term \hat{d} , shown in Fig. 10(a) allows for an online adaptation of the thermal system model and for an ongoing estimation of modeling errors and external disturbances. This term, inflated by the interval $[-\Delta d; +\Delta d]$, is directly used in the evaluation of the control law (35). In addition, the low-pass filtered temperature estimate $\hat{\vartheta}_{FC}$, following the measured data with good accuracy according to Fig. 10(b), is used in the evaluation of $[v]$.

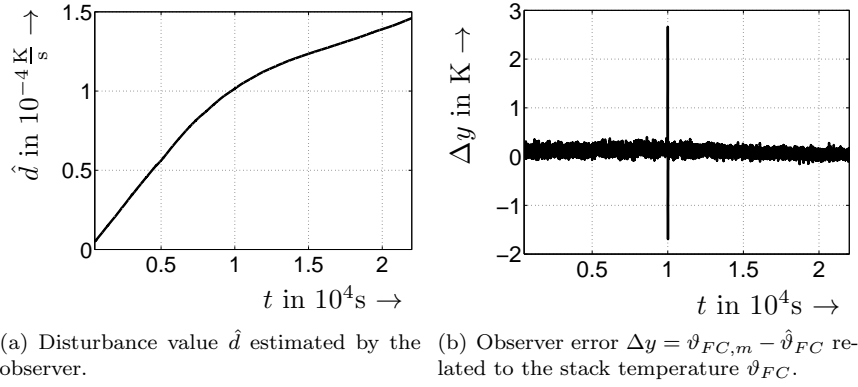


Figure 10: Experimental results of the disturbance observer for an estimation of the disturbance acting on the thermal behavior of the SOFC system.

5 Conclusions and Outlook on Future Work

In this paper, novel interval-based sliding mode control strategies have been derived which are capable of stabilizing the dynamics of uncertain models for SOFC systems in a guaranteed way. Besides a numerical verification of these procedures, an experimental validation has been performed for a test rig available at the Chair of Mechatronics at the University of Rostock. The implementation of the interval-based control procedure on the test rig has been performed under consideration of real-time constraints. These constraints were met by means of an implementation in C++ with the help of the interval library C-XSC. Moreover, the controller has been extended by a model-based disturbance observer which allows one to detect deviations between a point-valued system model and the actual system dynamics during control operation.

Future work will aim at the implementation of state estimation procedures with an improved spatial resolution of the stack module temperature. This can be achieved by a replacement of the global thermal system model by its semi-discretized version. A suitable sensitivity-based state estimation procedure has already been tested in offline simulations [14]. This estimator reconstructs the internal temperature distribution in an SOFC stack module from temperature measurements at a few selected positions, which are usually located at the stack module's inlet and outlet manifolds.

After a successful validation of this approach in experiments, we aim at the derivation of sliding mode approaches which allow for controlling the temperature at arbitrary positions in the interior of the stack module. Here, the case of controlling non-flat system outputs will be of special interest.

Finally, similarities between the design of interval-based sliding mode controllers as well as variable structure state observers will be investigated from a methodological point of view [16].

References

- [1] E. Auer, S. Kiel, and A. Rauh. Verified Parameter Identification for Solid Oxide Fuel Cells. In *Proc. of 5th Intl. Conference on Reliable Engineering Computing*,

- pages 41–55, Brno, Czech Republic, 2012. Available at http://rec2012.fce.vutbr.cz/documents/proceedings/REC2012_proceedings.pdf.
- [2] R. Bove and S. Ubertini, editors. *Modeling Solid Oxide Fuel Cells*. Springer, Berlin, 2008.
 - [3] T. Dötschel, E. Auer, A. Rauh, and H. Aschemann. Thermal Behavior of High-Temperature Fuel Cells: Reliable Parameter Identification and Interval-Based Sliding Mode Control. *Soft Computing*, 17(8):1329–1343, 2013.
 - [4] T. Dötschel, A. Rauh, and H. Aschemann. Reliable Control and Disturbance Rejection for the Thermal Behavior of Solid Oxide Fuel Cell Systems. In *Proc. of 7th Vienna Intl. Conference on Mathematical Modelling MATHMOD 2012*, Vienna, Austria, 2012. Available at ifac-papersonline.net.
 - [5] T. Dötschel, A. Rauh, L. Senkel, and H. Aschemann. Experimental Validation of Interval-Based Sliding Mode Control for Solid Oxide Fuel Cell Systems. In *Proc. of the European Control Conference ECC 2013*, pages 2489–2494, Zurich, Switzerland, 2013.
 - [6] A. Gubner. Non-Isothermal and Dynamic SOFC Voltage-Current Behavior. In S. C. Singhal and J. Mizusaki, editors, *Solid Oxide Fuel Cells IX (SOFC-IX): Volume 1 — Cells, Stacks, and Systems*, pages 814–826. The Electrochemical Society, 2005.
 - [7] W. Krämer. XSC Languages (C-XSC, PASCAL-XSC) — Scientific Computing with Validation, Arithmetic Requirements, Hardware Solution and Language Support, n.a. www.math.uni-wuppertal.de/~xsc/.
 - [8] H.J. Marquez. *Nonlinear Control Systems*. John Wiley & Sons, Inc., New Jersey, 2003.
 - [9] National Instruments. LABVIEW, 2013. <http://www.ni.com/labview/>.
 - [10] J.T. Pukrushpan, A.G. Stefanopoulou, and H. Peng. *Control of Fuel Cell Power Systems: Principles, Modeling, Analysis and Feedback Design*. Springer, Berlin, 2nd edition, 2005.
 - [11] A. Rauh and H. Aschemann. Parameter Identification and Observer-Based Control for Distributed Heating Systems – The Basis for Temperature Control of Solid Oxide Fuel Cells. *Mathematical and Computer Modelling of Dynamical Systems*, 18(4):329–353, 2012.
 - [12] A. Rauh, T. Dötschel, and H. Aschemann. Experimental Parameter Identification for a Control-Oriented Model of the Thermal Behavior of High-Temperature Fuel Cells. In *CD-Proc. of IEEE Intl. Conference on Methods and Models in Automation and Robotics MMAR*, Miedzyzdroje, Poland, 2011.
 - [13] A. Rauh, T. Dötschel, E. Auer, and H. Aschemann. Interval Methods for Control-Oriented Modeling of the Thermal Behavior of High-Temperature Fuel Cell Stacks. In *Proc. of 16th IFAC Symposium on System Identification SysID 2012*, pages 446–451, Brussels, Belgium, 2012.
 - [14] A. Rauh, L. Senkel, and H. Aschemann. Sensitivity-Based State and Parameter Estimation for Fuel Cell Systems. In *Proc. of 7th IFAC Symposium on Robust Control Design*, pages 57–62, Aalborg, Denmark, 2012.
 - [15] A. Rauh, L. Senkel, J. Kersten, and H. Aschemann. Verified Stability Analysis for Interval-Based Sliding Mode and Predictive Control Procedures with Applications to High-Temperature Fuel Cell Systems. In *Proc. of 9th IFAC Symposium on Nonlinear Control Systems*, pages 570–575, Toulouse, France, 2013.

- [16] L. Senkel, A. Rauh, and H. Aschemann. Interval-Based Sliding Mode Observer Design for Nonlinear Systems with Bounded Measurement and Parameter Uncertainty. In *CD-Proc. of IEEE Intl. Conf. on Methods and Models in Automation and Robotics*, Miedzyzdroje, Poland, 2013.
- [17] B.J. Spivey, J.D. Hedengren, and T.F. Edgar. Constrained Control and Optimization of Tubular Solid Oxide Fuel Cells for Extending Cell Lifetime. In *Proc. of the American Control Conference ACC 2012*, pages 1356–1361, Montréal, Canada, 2012.
- [18] Ch. Stiller. *Design, Operation and Control Modelling of SOFC/GT Hybrid Systems*. PhD thesis, University of Trondheim, 2006.
- [19] Ch. Stiller, B. Thorud, O. Bolland, R. Kandepu, and L. Imsland. Control Strategy for a Solid Oxide Fuel Cell and Gas Turbine Hybrid System. *Journal of Power Sources*, 158:303–315, 2006.
- [20] K. Sundmacher, A. Kienle, H.J. Pesch, J.F. Berndt, and G. Huppmann, editors. *Molten Carbonate Fuel Cells. Modeling, Analysis, Simulation, and Control*. Wiley-VCH, Weinheim, 2007.
- [21] The MathWorks, Inc. MATLAB/ SIMULINK, 2013. <http://www.mathworks.com>.
- [22] V.I. Utkin. *Sliding Modes in Control and Optimization*. Springer-Verlag, Berlin, Heidelberg, 1992.
- [23] V.I. Utkin. Sliding Mode Control Design Principles and Applications to Electric Drives. *IEEE Transactions on Industrial Electronics*, 40(1):23–36, 1993.